

Double-shelled hollow mesoporous silica incorporated copper (II) (Cu/DS-HMS-NH₂) as a catalyst to promote in-situ esterification/transesterification of low-quality palm oil

Antonius Nova Rahadi¹ | Jeremia Jonathan Martinus¹ |
 Shella Permatasari Santoso^{1,2} | Maria Yuliana¹  | Alfin Kurniawan³ |
 Chintya Gunarto² | Sandy Budi Hartono¹ | Felycia Edi Soetaredjo^{1,2} |
 Suryadi Ismadji^{1,2}

¹Department of Chemical Engineering,
 Widya Mandala Surabaya Catholic
 University, Surabaya, Indonesia

²Department of Chemical Engineering,
 National Taiwan University of Science
 and Technology, Taipei, Taiwan

³Department of Chemistry, National Sun
 Yat-Sen University, Kaohsiung, Taiwan

Correspondence

Maria Yuliana, Department of Chemical
 Engineering, Widya Mandala Surabaya
 Catholic University, Kalijudan
 37, Surabaya 60114, Indonesia.
 Email: mariayuliana@ukwms.ac.id

Funding information

Widya Mandala Surabaya Catholic
 University, Grant/Award Number: 2263/
 WM01/N/2020; National Taiwan
 University of Science and Technology;
 National Sun Yat-Sen University

Summary

To encourage the utilization of low-quality palm oil with high free fatty acid and moisture content (>0.1 wt%), a novel catalyst with two spatial shells and different active sites, double-shelled hollow mesoporous silica incorporated copper (II) (Cu/DS-HMS-NH₂), is fabricated via the two-stage hydrolysis and condensation technique. The influence of four parameters (eg, catalyst loading, temperature, reaction time, and the mass ratio of methanol to degummed palm oil (DPO)) on the yield of fatty acid methyl ester (FAME) are monitored and optimized using a combination of response surface methodology (RSM) and face centered-central composite experimental design (CCF-CCD). The optimized FAME yield is predicted at 86.63 wt% and experimentally obtained at 87.14 ± 0.11 wt% (FAME purity of 98.45 ± 0.67 wt%) under the following optimum condition: 55.3°C, 5 h, methanol to DPO mass ratio of 5.3:1, and 5 wt% catalyst loading. The experimental and predicted values are proportional and in direct agreement with an error of 0.51%. The goodness of fit analysis also indicates conformity between the mathematical model and the experimental results. The reusability study shows that Cu/DS-HMS-NH₂ is stable until the fifth run, evident from the yield of FAME which stays above 80%. These results prove the potential utility of Cu/DS-HMS-NH₂ for the direct conversion of low-quality vegetable oils to biodiesel without any pre-treatment.

KEYWORDS

bifunctional catalyst, biodiesel, double-shelled, mesoporous silica, optimization study

Abbreviations: CPO, crude palm oil; DPO, degummed palm oil; FAME, fatty acid methyl esters; FFA, free fatty acids; MSN, mesoporous silica nanoparticles; S-HMS-NH₂, single-shelled hollow mesoporous silica.

Antonius Nova Rahadi and Jeremia Jonathan Martinus contributed equally to this work.

1 | INTRODUCTION

The ever-increasing dependency on fossil fuel as an energy source may endanger its sustainability. At the same time, the long-term use of this fuel also raises an environmental concern because its flue gas emission

contains various greenhouse gases (ie, CO₂, CH₄, N₂O, and O₃).¹ The development of sustainable and environmentally benign alternative fuels is, therefore, urgently required. Among the available alternative fuels, biodiesel is known to be environmentally friendly as it possesses a high oxygen content, which can increase the fuel combustion rate, and reduce carbon monoxide production.^{2,3} Currently, the mass production of biodiesel uses the conventional base catalysts, such as sodium methylate and potassium hydroxide, since they provide a high reaction rate and satisfactory yields. However, these homogenous catalysts require several additional post-separation steps (eg, acid washing, separation, and refining) for biodiesel purification, exhibit poor tolerance to contaminants (free fatty acids [FFA] and moisture),⁴ and are not reusable.⁵ Hence, the use of this type of catalyst limits the selection of feedstock materials and increases the overall production cost.

On the other hand, heterogeneous catalysts offer several advantages over their homogeneous counterparts due to their reusability, insensitivity to impurities in the feedstock, and easier separation from the reaction product.⁶ Many studies have reported the synthesis of biodiesel using heterogeneous acid or base solid catalysts for producing biodiesel,^{6,7} such as metal-organic frameworks^{8,9} and functionalized mesoporous silicas.^{5,10} A wide variety of solid catalyst, for example, alkaline-modified zirconia,¹¹ polyoxometalate (POM)-based sulfonated ionic liquid immobilized-UiO-66-2COOH,¹² Amberlyst-15 and its modified form,¹³ carbon nanotube-based solid sulfonic acids,¹⁴ sulfated niobium oxide,¹⁵ and solid superacid catalyst (SO₄²⁺/ZrO₂-TiO₂/La³⁺),¹⁶ has been studied. However, despite their insensitivity to impurities and ability to perform simultaneous reactions, these catalysts require extreme reaction conditions, with the temperature range between 100 and 250°C. Amberlyst-15 and POM-based sulfonated ionic liquid immobilized-UiO-66-2COOH also require a long reaction time (up to 9 h)¹³ and high catalyst loading (up to 10 wt%),¹² respectively.

In recent years, mesoporous silica nanoparticles (MSN) have gained extensive attention in many applications, due to their low cost, facile synthesis, ease of surface modification, considerable pore capacity, various particle frameworks, and tunable textural properties.¹⁷⁻¹⁹ García-Sancho et al (2011)²⁰ reported the use of niobium-containing MCM-41 to produce biodiesel from edible sunflower oil, while Xie et al (2015)⁷ studied the performance of SBA-15 immobilized with 1,3-dicyclohexyl-2-octylguanidine, to prepare commercial soybean oil-based FAME. While both MCM-41 and SBA15 possess excellent textural properties, for example, high surface area and good porosity, it requires complicated synthesis procedures

to design two spatial shells with different active sites within a particle of the two materials, as both have rod-like structure. This hinders the impregnation of two active components on the surface of MSN, and therefore, limits its use in the synthesis of biodiesel from low-quality oils.

In this study, we design a new class of catalyst, the copper-incorporated double-shelled hollow mesoporous silica (Cu/DS-HMS-NH₂), with distinct functionalities that can facilitate both esterification and transesterification reactions simultaneously in one simple process with mild reaction conditions. While the inner layer is purposely designed to promote the transesterification reaction by adding -NH₂ as the basic site in the fabrication, while the outer layer is impregnated with copper (Cu (II)) to induce the esterification reaction. The copper metal is mainly used as an active site for the esterification reaction due to its availability and high reactivity to various types of reactions. The incorporation of copper to the DS-HMS-NH₂ surface also increases the thermal stability of the catalyst and improves the esterification efficiency in converting the FFA to fatty acid methyl ester (FAME).^{8,21} Therefore, it is certainly of great interest to study the catalytic performance of Cu/DS-HMS-NH₂, as this bifunctional catalyst improves the chance of low-quality oil to be widely utilized as the raw material for biodiesel production, and at the same time, offers an ability to promote the concurrent esterification/transesterification reaction in a one-pot synthesis.

The utilization of low-quality oils for biodiesel production has attracted public attention, as it may sustain the supply chain of the food sector. Various feedstocks, for example, animal fats,^{22,23} waste cooking oil,²⁴ leather tanning waste,²⁵ and jatropha (*Jatropha curcas* L.) oil,²⁶ have been developed to prepare commercial-grade biodiesel. The present research tests the catalytic ability of Cu/DS-HMS-NH₂ to produce biodiesel from degummed palm oil (DPO) in several operating variations (catalyst loading (wt%), temperature (°C), the mass ratio of methanol to DPO, and reaction time (h)). With the high amount of FFA and moisture, DPO is regarded as a low-quality oil; therefore, it is considered as a suitable raw material to determine the viability of Cu/DS-HMS-NH₂ for the conversion of both FFA and triglycerides in DPO into biodiesel. The selection of DPO is also to avoid food shortages, simplify the process and lower the operational cost. The process evaluation and optimization are determined using a response surface methodology (RSM) approach combined with face centered-central composite experimental design (CCF-CCD). The reusability of Cu/DS-HMS-NH₂ is then investigated at the optimum operating condition. Moreover, the catalytic reaction mechanism of the in-situ esterification/transesterification

during the conversion of DPO to biodiesel using Cu/DS-HMS-NH₂ is also discussed.

2 | MATERIALS AND METHODS

2.1 | Materials

All chemicals used in this study were of reagent grade and purchased from Sigma-Aldrich (Germany). Therefore, they were used without further purification. Meanwhile, the raw lipid material, crude palm oil (CPO), was obtained from PT. Batarra Elok Semesta Terpadu, a local palm oil manufacturer in Indonesia. Prior use, CPO was subjected to the degumming process: CPO and phosphoric acid (PA) with a ratio of 100:1 (v/v) were mixed and heated to 80°C, where the temperature of the system was maintained isothermally for 15 min. The mixture was then cooled down to room temperature and subsequently subjected to centrifugation at 4900 rpm for 10 min to remove the gum soluble in the PA-rich phase. To ensure the remnants of gum in CPO were completely removed, a 2-portion of hot water was added to one-portion of CPO. The mixture was vigorously mixed using a high-speed agitation system before subjected to another centrifugation process (4900 rpm, 10 min) to obtain the DPO. Both CPO and DPO were analyzed for their FFA, acid value, saponification value, and moisture content using the standard method of AOCS Ca 5a-40, Cd 3d-63, Cd 3d-25, and Ca 2e-84, respectively. The fatty acid profile in DPO was also observed using GC-2014 (Shimadzu Ltd., Japan) equipped with Restek Rtx-65TG (30 m × 0.25 mm ID × 0.10 μm film thickness, Restek) and a flame ionization detector (FID). The average molar weight of CPO and DPO (M_{PO}) was calculated by Equation (1), where SV and AV are corresponding to the saponification value (mg KOH/g oil) and acid value (mg KOH/g oil) of the oil.

$$M_{PO} = \frac{56.1 \times 1000 \times 3}{(SV - AV)}. \quad (1)$$

2.2 | Synthesis of Cu/DS-HMS-NH₂

The single-shelled hollow mesoporous silica (S-HMS-NH₂) was prepared in accordance with the procedures reported by Wang et al (2015),²⁷ where a mixture of CTAB (0.14 g), ethanol (20 mL), deionized water (50 mL), and ammonia solution 25% (1 mL) was introduced into a beaker and stirred for 15 min at room temperature. One milliliter of tetraethyl orthosilicate (TEOS) was then slowly added to the mixture and kept stirring

for 24 h. The pH during the synthesis was monitored at 10-11. The white precipitates were separated via centrifugation at 4500 rpm for 30 min, ethanol washing, and drying at 120°C overnight. The resulting dried solid was calcined at 550°C for 6 h to obtain S-HMS-NH₂.

Meanwhile, the fabrication of the second shell was conducted using the modified methods of You et al (2018)²⁸: 0.5 g CTAB was dissolved in 18 mL deionized water and 50 mL ethanol. Then, 4 mL deionized water, 0.063 g S-HMS-NH₂, and 8.5 mL 25% ammonia solution were added into the solution. A 100 μL of TEOS and 21 μL of APTES were subsequently added to the above solution at room temperature to induce the condensation of silica. The reaction system was maintained homogeneous for 24 h under continuous agitation; the same pH range (pH = 10-11) was observed. After the reaction was completed, the mixture was centrifuged at 4500 rpm for 10 min to obtain the solid phase, which was repeatedly washed with ethanol. The sample was dried at 100°C overnight to remove the solvent. To eliminate the surfactant from mesoporous material, the sample was calcined at 550°C for 6 h to obtain DS-HMS-NH₂ particles.

The impregnation of Cu (II) to DS-HMS-NH₂ particles was carried out using the traditional wet impregnation method studied by Zaidi and Pant (2008)²⁹ with few modifications. A 0.1 g DS-HMS-NH₂ was dissolved into 0.001 M CuSO₄ solution and reacted for 12 h at constant pH (5.0). The solid phase was separated by centrifugation at 4500 rpm for 10 min, oven-dried for 12 h at 100°C, and calcined for 5 h at 550°C to yield Cu/DS-HMS-NH₂ particles with 1 wt% of impregnated Cu (II).

2.3 | Experimental design and process optimization

The biodiesel synthesis through an in-situ esterification/transesterification reaction between methanol and DPO using the heterogeneous catalyst of Cu/DS-HMS-NH₂ was conducted in various conditions, namely reaction temperature, time, and the mass ratio of DPO to methanol. These experiments were conducted at a constant catalyst loading that gives the highest amount of FAME yield. These independent factors were selected based on their relevance to the process efficiency and economic applicability. A design of experiment (DOE), combined with the standard design tools, face-centered central composite design (CCF-CCD), and RSM, was employed to determine the optimum operating condition for the synthesis of biodiesel with the FAME yield selected as the response. The three optimized variables were divided into the following coded level: low (−1), middle (0), and high (+1), as presented in Table 1.

The designed matrix between the encoded variables, the predicted and experimental responses are presented in Table 2. Triplicated experiments were carried out for every set of the input parameter to generate a good response reproducibility. Seven experimental data at the center point (0,0,0) were presented individually for every run. The responses were fitted into a second-order polynomial model, developed using a 3-way analysis of variance (ANOVA) with a 95% confidence level. The goodness-of-fit of the mathematical model was evaluated by various parameters, including the coefficient of determination (R^2), the lack-of-fit sum of squares, coefficient of variations (C.V.), and adequate precision. The surface plots between the two inter-correlated variables were

developed using the regressed experimental results by maintaining one variable constant in the middle point while changing the other two variables.

The correlation between the predicted response (yield of FAME, wt%) and the independent variables are expressed by Equation (2), where Y is the predicted FAME yield (wt%); k_0 , k_i , k_{ii} , k_{ij} are the regression coefficients for the intercept, linear, quadratic, and interactions of the independent variables, respectively; X_i and X_j are the coded factors (A, B, C).

$$Y = k_0 + \sum_{i=1}^3 k_i X_i + \sum_{i=1}^3 k_{ii} X_i^2 + \sum_{i=1}^3 \sum_{j=1}^3 k_{ij} X_i X_j. \quad (2)$$

Reaction parameter	Coded factor	Factor level		
		-1	0	+1
Temperature (°C)	A	45	55	65
Reaction time (h)	B	1	3	5
Mass ratio of methanol to DPO	C	2:1	4:1	6:1

TABLE 1 The coded parameters with their actual values in the design of the experiment

Run	Input parameters			Responses (yield of FAME, wt%)	
	A	B	C	Experimental (n = 3)	Predicted
1	-1	-1	-1	52.94	52.87
2	-1	-1	1	59.68	59.39
3	-1	0	0	73.48	73.52
4	-1	1	-1	76.85	76.65
5	-1	1	1	80.46	80.97
6	0	-1	0	65.82	66.97
7	0	0	-1	72.85	73.81
8	0	0	0	80.49	79.95
9	0	0	0	79.81	79.95
10	0	0	0	81.42	79.95
11	0	0	0	80.86	79.95
12	0	0	0	79.27	79.95
13	0	0	0	78.85	79.95
14	0	0	0	80.85	79.95
15	0	1	0	85.68	85.49
16	1	-1	-1	58.75	58.00
17	1	-1	1	68.95	68.91
18	1	0	0	75.77	76.69
19	1	1	-1	73.42	73.47
20	1	1	1	82.35	82.17

TABLE 2 The experimental design based on CCF-CCD, presented along with the experimental and predicted responses

2.4 | The synthesis of biodiesel using Cu/DS-HMS-NH₂ as a heterogeneous catalyst

The reaction was carried out in a flask, equipped with a heating mantle, and reflux condenser, under atmospheric pressure. Methanol and DPO were initially introduced into the flask in various mass ratios (2:1, 4:1, and 6:1). The mixture was stirred and heated to the desired temperature (45, 55, and 65°C) before the addition of Cu/DS-HMS-NH₂ to the system (1, 3, 5, and 7 wt% of the DPO). The system was maintained homogenous under constant agitation (250 rpm) throughout the reaction (1, 3, and 5 h). Once the reaction reached completion, Cu/DS-HMS-NH₂ was removed from the mixture by filtration to obtain the two-layered product, which was subsequently subjected to an overnight liquid-liquid separation using n-hexane. The light phase contains n-hexane and FAMES, while the heavy phase was rich in glycerol, excess methanol, and other by-products. The bottom layer was repeatedly washed by n-hexane to ensure that all FAME has been extracted. The obtained FAME-rich phase was then subjected to a solvent removal using an IKA RV 10B vacuum evaporator to obtain a purified final product. The yield of FAME can be expressed by the following equation:

$$\text{Yield of FAME (\%)} = \frac{P_{\text{FAME}} \times m_{\text{BD}}}{m_{\text{DPO}}} \times 100\%, \quad (3)$$

where P_{FAME} (%) is the purity of FAME obtained from Equation (4), m_{BD} (g) is the mass of the final biodiesel product obtained from the in-situ esterification/trans-esterification reaction process, and m_{DPO} (g) is the mass of DPO used in the reaction.

2.5 | Characterization

The catalyst characterization includes scanning electron microscopy (SEM), transmission electron microscopy (TEM), energy-dispersive X-ray spectroscopy (EDX), nitrogen sorption, and thermogravimetric analysis (TGA) to respectively determine the morphology; pore and double-shelled structure; elemental composition; textural properties; and thermal stability of Cu/DS-HMS-NH₂. SEM and EDX images were taken on a JEOL JSM-6500 F (Jeol Ltd., Japan) running at 15.0 kV accelerating voltage and 12.2–12.5 mm working distance. TEM images were acquired using JEOL JEM-3010 with an accelerating voltage of 200 kV. The nitrogen sorption analysis was carried out at 77 K on a Micrometrics ASAP 2010 Sorption Analyzer. Before analysis, the samples were outgassed at

150°C for 4 h under vacuum. The adsorption-desorption of nitrogen isotherm is run at a pressure range (p/p°) of zero to unity. To analyze the catalyst stability at high temperatures, TGA analysis was employed on a TG/DTA Diamond instrument (Perkin-Elmer, Japan). A certain mass of the sample was placed in a platinum pan and heated from the ambient temperature to 900°C with a heating rate of 10°C/min to monitor the thermal stability of the catalyst. Nitrogen gas was purged into the system at the rate of 20 mL/min throughout the entire analysis to maintain the system oxygen-free.

To verify the formation of FAME from the DPO, the functional groups of DPO and FAME were analyzed using Shimadzu FTIR 8400 s in the wavenumber range of 4000–400 cm⁻¹. Then, the purity and compositional analysis of FAME were conducted using Shimadzu GC-2014 (Shimadzu, Japan), according to the method reported by Santosa et al (2019).²³ The FAME purity in the sample was calculated following Equation (4) below, where $\sum A_{\text{FAME}}$ is the total area of FAME peaks, A_{MH} is the peak area of methyl heptadecanoate (MH), V_{MH} is the volume of MH solution added to the sample (ml), C_{MH} is the actual concentration of MH solution (g/ml), and m_{BD} is the sample weight of the final biodiesel product (g).

$$\begin{aligned} \text{FAME Purity } (P_{\text{FAME, wt\%}}) \\ = \left(\frac{\sum A_{\text{FAME}} - A_{\text{MH}}}{A_{\text{MH}}} \times \frac{V_{\text{MH}} C_{\text{MH}}}{m_{\text{BD}}} \right) \times 100\%. \end{aligned} \quad (4)$$

2.6 | Reusability study

The reusability study was performed by repeatedly using Cu/DS-HMS-NH₂ for the preparation of biodiesel at the optimum reaction condition. After each reaction cycle, Cu/DS-HMS-NH₂ was recovered by centrifugation (4500 rpm, 15 min) and calcination (550°C, 5 h) to be subsequently reused. Meanwhile, fresh DPO and methanol were used in every cycle. The repetition was conducted until the FAME yield became lower than 80 wt%. The purity and yield of FAME were measured using the procedure in Sections 2.4 and 2.5.

3 | RESULTS AND DISCUSSIONS

3.1 | Characterization of Cu/DS-HMS-NH₂

As presented in Figure 1, the synthesis route of Cu/DS-HMS-NH₂ can be divided into several steps as follows: (1) the ellipsoidal micelles of CTAB are formed with an

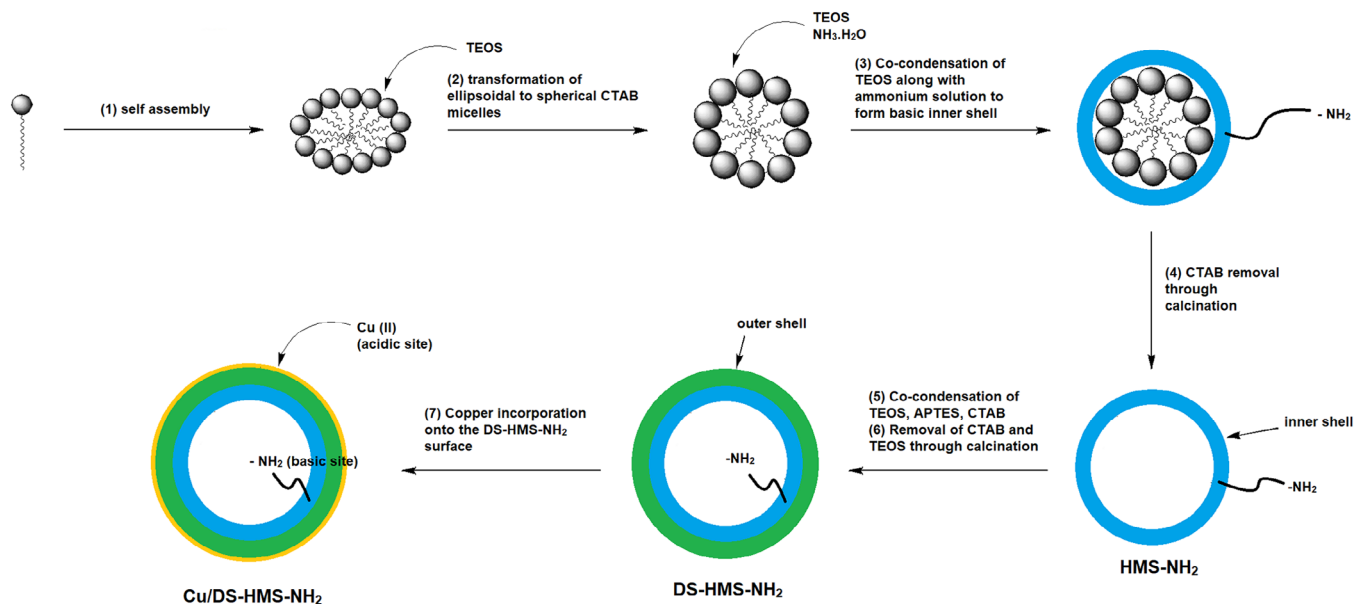


FIGURE 1 Fabrication route of Cu/DS-HMS-NH₂ [Colour figure can be viewed at wileyonlinelibrary.com]

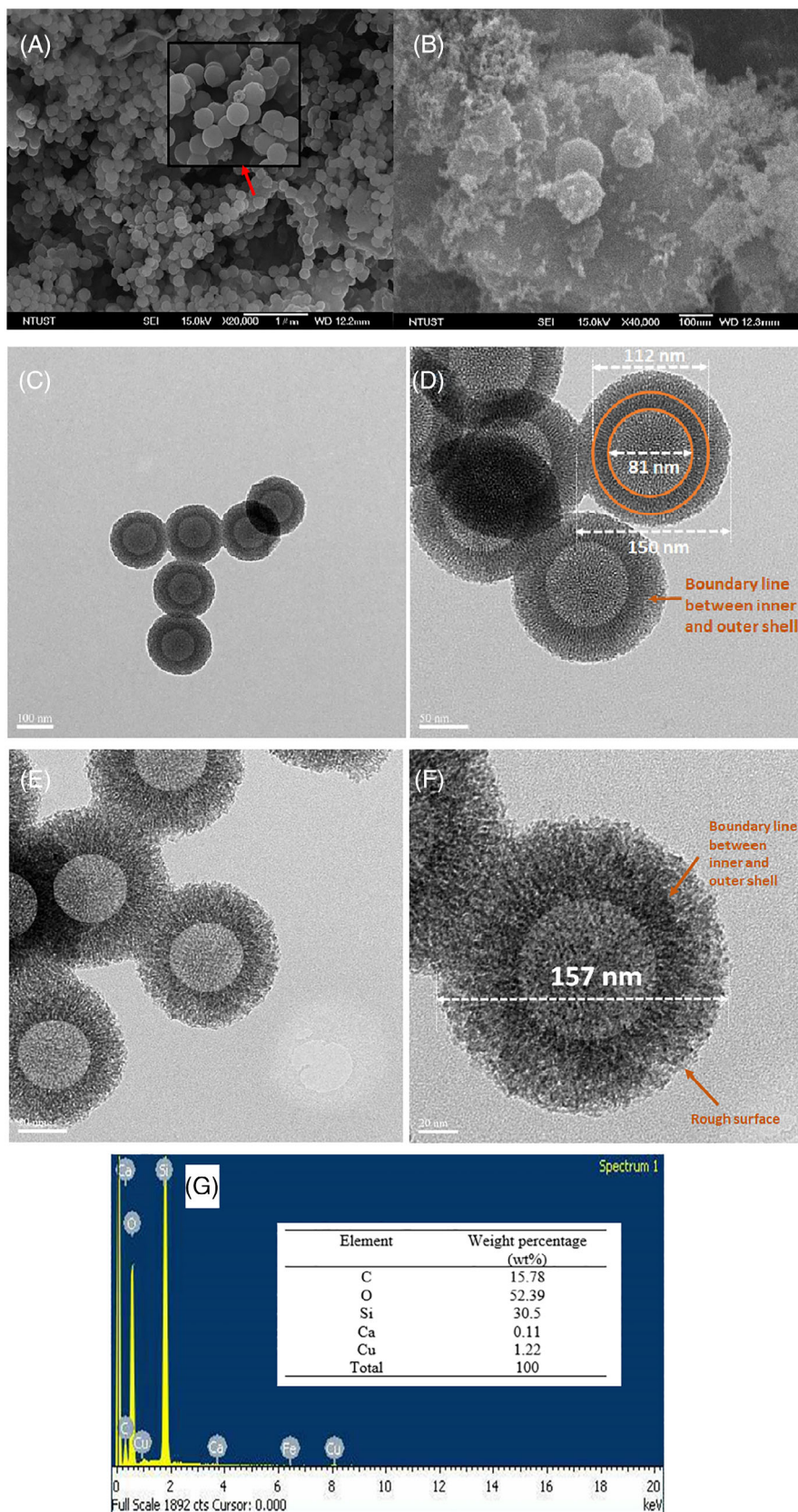
inner core consisting of the hydrophobic tail, (2) during the addition of TEOS, the micelles enlarge, and result in the transformation of micelle shape from ellipsoidal to spherical, (3) TEOS has then undergone hydrolysis and condensation reaction along with the ammonium solution to form a silica shell around the micelles, (4) the CTAB micelles are removed from the core using calcination to form HMS-NH₂, (5) to synthesize the outer shell and create the DS-HMS-NH₂, TEOS, APTES, and CTAB are subjected for another hydrolysis and condensation reaction, (6) Again, both CTAB and APTES are removed from the DS-HMS-NH₂ nanospheres by calcination at high temperature, and (7) Cu (II) are impregnated on the surface of DS-HMS-NH₂ using wet impregnation technique to produce Cu/DS-HMS-NH₂.

The morphological structure of the fabricated catalyst (Cu/DS-HMS-NH₂) powder is analyzed using SEM and TEM analysis (Figure 2). Figure 2A,B captures the respective surface morphology of DS-HMS-NH₂ and Cu/DS-HMS-NH₂ particles. Due to the spontaneous formation through co-condensation during the synthesis, both particles are found to be spherical in shape, uniform in size (at ~150 nm), and have a neat surface structure.²⁷ Spherical particle shape was also reported by You et al (2018)²⁸ for a similar double-shelled hollow mesoporous silica. As seen from the corresponding figures, there is a clear difference between DS-HMS-NH₂ and Cu/DS-HMS-NH₂, particularly in their surface roughness. It is apparent from Figure 2B that Cu/DS-HMS-NH₂ possesses a rough surface topography because of the impregnation of copper nanoparticles, which shapes including rods, cubes, and tetrahedrons. The TEM images (Figure 2C-F)

confirm the formation of the double-shell, where the inner shell has a higher silica density than the outer one, indicated by the darker color gradation. Figure 2D shows that both the inner and outer shells of DS-HMS-NH₂ have a similar thickness, approximately 16-19 nm. It also verifies that DS-HMS-NH₂ has a diameter of 150 nm, with a hollow core size of 81 nm. Meanwhile, Figure 2F shows that the Cu/DS-HMS-NH₂ possesses a diameter of 157 nm, slightly larger than the not-impregnated particles, indicating that copper incorporation onto the surface adds some layer, with approximately 7 nm in thickness. The copper impregnation is further verified by the results of the EDX analysis (Figure 2G). It can be seen from the elemental composition that there is 1.22 wt% of impregnated copper on the particle surface, which meets the expected copper content in the Cu/DS-HMS-NH₂ catalyst. The other elemental content includes (1) 30.5 wt% silica and 52.39 wt% oxygen which are the main elements constructing silica nanoparticles, (2) 15.78 wt% carbon which comes from the undegraded TEOS and/or surfactant, and (3) trace amount of calcium (0.11 wt%).

The adsorption-desorption isotherm of Cu/DS-HMS-NH₂ (Figure 3A) implies that this catalyst possesses a typical type-IV mesoporous isotherm,^{30,31} indicating the presence of mesoporous capillary pores within the particles, with the mean pore diameter of 2.43 nm. Khatun et al (2017)³² reported similar adsorption-desorption profile for the mesoporous particle, where only a gradual increase in nitrogen adsorption occurs in the p/p^0 range from 0.1 to 0.9, while a sharp increase was observed in the range of p/p^0 between 0-0.1 and 0.9-1.0. Another study mentioned that a steep increase at p/p^0 close to unity also suggests

FIGURE 2 A, SEM image of DS-HMS-NH₂; B, SEM image of Cu/DS-HMS-NH₂; C, and D, TEM image of DS-HMS-NH₂; E, and F, TEM images Cu/DS-HMS-NH₂; and G, EDX image of Cu/DS-HMS-NH₂ [Colour figure can be viewed at wileyonlinelibrary.com]



that there are macropores interior in the particle, which corresponds to the hollow structure.³³ An identical hysteresis loop between the adsorption and desorption curves

indicates the same sorption tendency and behavior indicates the same sorption tendency and behavior between the two, emphasizing that this catalyst possesses high accessibility.¹⁰ The textural properties of Cu/DS-

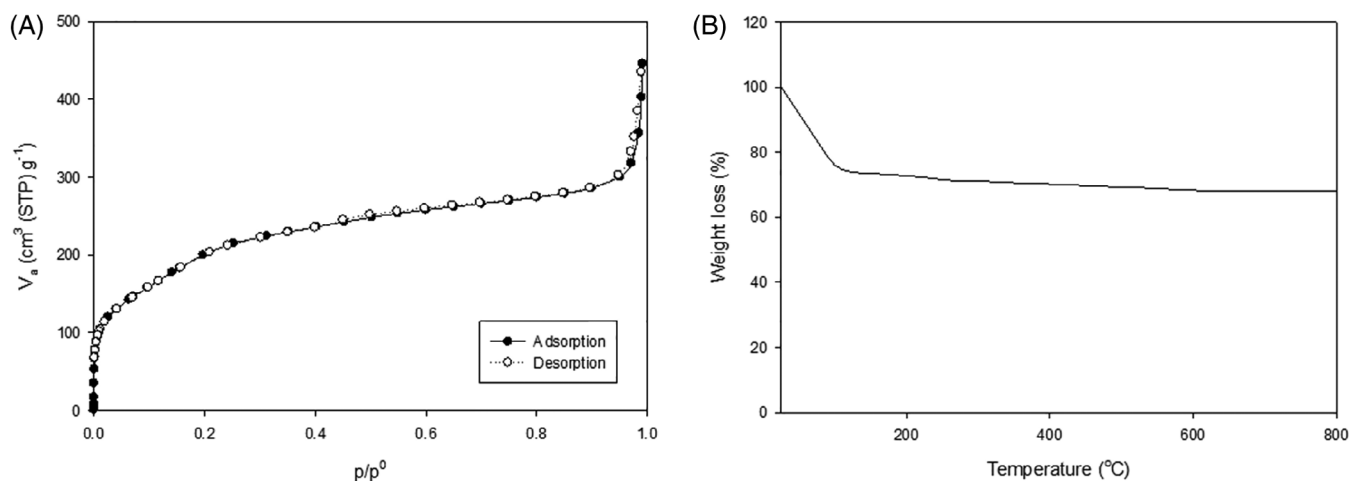


FIGURE 3 A, N_2 adsorption/desorption isotherm and B, TGA profile of Cu/DS-HMS-NH₂

HMS-NH₂ (surface area, S_{BET} , and pore volume, V_p) are monitored at 733.24 m²/g and 0.54 cm³/g. This result shows that the catalyst possesses comparable, if not higher, textural properties to the existing heterogeneous catalysts used for biodiesel production which generally range from 200 to 1300 cm²/g for the S_{BET} , and from 0.18 to 1.68 cm³/g for the V_p .^{8,28,34,35}

Figure 3B presents the degree of thermal stability of the catalyst which is determined through TGA analysis. The figure shows that a weight loss of 23 wt% occurs in the temperature range of 0 to 100°C. This is likely due to the dehydration and removal of the hydroxyl groups from the surface of the particles. At a temperature higher than 100°C, the catalyst particles do not experience significant weight loss, implying that surfactants and the other organic compounds have been removed in the previous calcination process³⁶; thus, it can be concluded that Cu/DS-HMS-NH₂ has good thermal stability.

3.2 | The effect of the reaction parameters on the yield of FAME in the biodiesel preparation using Cu/DS-HMS-NH₂

Table 3 summarizes the characteristics of CPO and DPO used in biodiesel production using Cu/DS-HMS-NH₂. Notably, DPO possesses high FFA content (5.54 wt%), rendering the lipid material a low-quality oil. Figure 4 shows the influence of the catalyst loading on the yield of FAME. Based on the figure, it can be seen that the in-situ esterification/transesterification is significantly affected by the amount of catalyst used. Escalating the Cu/DS-HMS-NH₂ loading from 1 wt% to 5 wt% greatly improves the yield of FAME by more than 10 folds. However, a

TABLE 3 Characteristics of CPO and DPO

Parameter	CPO	DPO
FFA (wt%)	5.68	5.54
Acid value ($\frac{mg\ KOH}{g\ DPO}$)	12.13	12.04
Moisture (wt%)	0.51	0.57
Fat content (wt%)	93.18	93.65
Saponification value ($\frac{mg\ KOH}{g\ DPO}$)	232.23	234.08
Molar weight ($\frac{g}{mol}$)	764.65	756.62
Fatty acid profile (wt%)	-	
Lauric acid (C12:0)		0.9
Myristic acid (C14:0)		1.4
Palmitic acid (C16:0)		43.7
Stearic acid (C18:0)		3.4
Oleic acid (C18:1)		38.3
Linoleic acid (C18:2)		11.2
Linolenic acid (C18:3)		0.7
Arachidic acid (C20:0)		0.4

further catalyst addition to 7 wt% slightly reduces the FAME yield. Previous studies agree that the catalyst amount above 7.5 wt% is inefficient and instead, reduces the yield.^{5,37-39} This is because the higher the content of solid catalyst added to the reaction system, the higher the mixture viscosity, leading to an inconsistent dispersity. Gurunathan and Ravi (2015)¹ added that a high amount of catalyst inhibited the interaction of reactant with the active sites of the catalyst due to aggregation; therefore, lowers the FAME yield.

Figure 5A(1-3) presents the effect of two interconnected variables on the experimental FAME yield, in

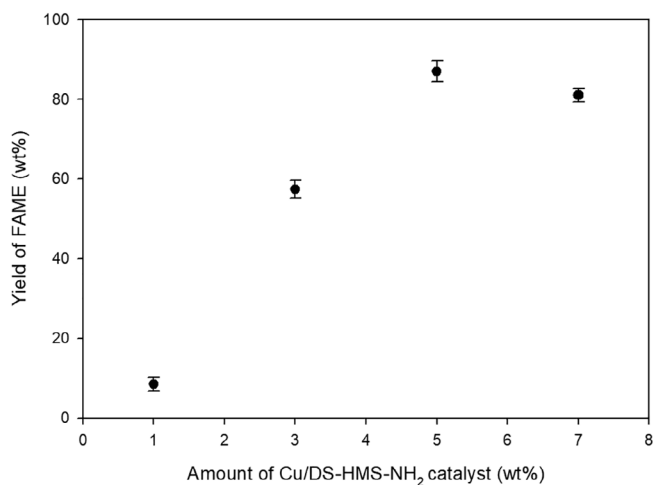


FIGURE 4 The effect of Cu/DS-HMS-NH₂ loading (wt%) on the yield of FAME (wt%) (reaction time = 5 h, temperature = 65°C, and mass ratio of methanol to DPO = 6:1)

3D surface plots. The effect of reaction time on the yield of FAME is depicted in Figures 5A(1,2). Looking at the data curve, it is apparent that reaction time gave a significant influence on the yield of FAME. An increase in the duration of reaction from 1 to 5 h sharply escalates the response. Longer reaction time gives the reactants higher opportunities to come into contact with the active sites of Cu/DS-HMS-NH₂.⁴⁰ It also allows the adsorption and diffusion of the reactants to reach the internal pores of the catalyst, where the actual reactions took place. In terms of the catalyst, extending the reaction time also provides the catalyst more time to adsorb the reactant and desorb the product.⁸ Moreover, as the sorption of reactant from the catalyst is the reaction governing step,⁴¹ allowing longer contact between both reactants and catalyst assures high conversion of DPO to FAME.

The effect of reaction temperature on the other two variables is depicted in Figure 5A(1,3). Both esterification and transesterification reactions are endothermic and reversible process.^{42,43} Therefore, it can be seen that when the temperature is increased from 45°C to 55°C, a significant increase is observed in the yield of FAME. Heating the reaction system accelerates the mobility of the reactant molecules and catalyst particles, leading to intensive particle collision in the system. This phenomenon increases the reaction rate constant and shifts the reaction to the right (product side).⁴³⁻⁴⁶ From another viewpoint, an increase in temperature also enhances the mass transfer and diffusivity of the reactant molecules to the pore of Cu/DS-HMS-NH₂; therefore, heightening the yield of FAME. A further increase to the temperature of 65°C, on the other hand, lowers the yield of FAME. Madhuvilakku and Piraman (2013) and Yin et al (2016)^{47,48} stated that this tendency occurs due to the loss

of methanol in the reaction system caused by evaporation, which induces the reverse reaction towards the reactants.

A similar trend is also observed for the influence of methanol to DPO mass ratio on the FAME yield. As seen from Figure 5A(2,3), increasing the level of methanol to DPO mass ratio from 2:1 to 4:1 escalates the FAME yield, while further addition of methanol in the system, reaching the methanol to DPO mass ratio of 6:1, gives an antagonistic effect to the yield. This result is in accordance with the study proposed by Gunawan et al (2014)⁴⁹ where the excess methanol is favorable to the reaction, only to a certain extent. Pangestu et al (2019)⁸ added that even though the yield of FAME may increase along with the amount of methanol, it may as well rapidly improve glycerol production. This phenomenon may subsequently provoke a reverse reaction to the reactant side, lowering the FAME yield. Furthermore, a higher mass ratio of methanol to DPO will only increase the production cost, reducing the operating efficiency.²³

3.3 | Process optimization

RSM is statistically employed to determine the optimum operating conditions for the production of FAME using Cu/DS-HMS-NH₂, by simultaneously integrating the three important parameters, for example, reaction time, temperature, and the mass ratio of methanol to DPO. Table 2 presents the correlation between the input variables and their corresponding response (FAME yield, wt%). The average SE estimate between the actual and predicted response is obtained at 0.01% (n = 20), indicating sufficient data accuracy. A similar trend as the experimental data is also observed from the predicted plots, as depicted in Figure 5B(1-3).

The statistical analysis to determine the significance of the three independent variables on the yield of FAME is conducted using ANOVA, with the α value set at 0.05 to minimize the analysis error; and the results are presented in Table 4. All linear terms and the interaction between reaction temperature and the mass ratio of methanol to DPO are observed to have a positive effect on the FAME yield, while in contrast, the quadratic coefficients and the other two interactions give an antagonistic effect to the yield of FAME.

It can be seen from Table 4 that all terms, except the interaction between reaction time and the mass ratio of methanol to DPO (BC), show prominence to the FAME yield (P value < 0.05). Based on the perturbation plot presented in Figure 6A, reaction time (B) is regarded as the most dominant contributor, where the plotline rises the steepest compared to the other variables. It is successively

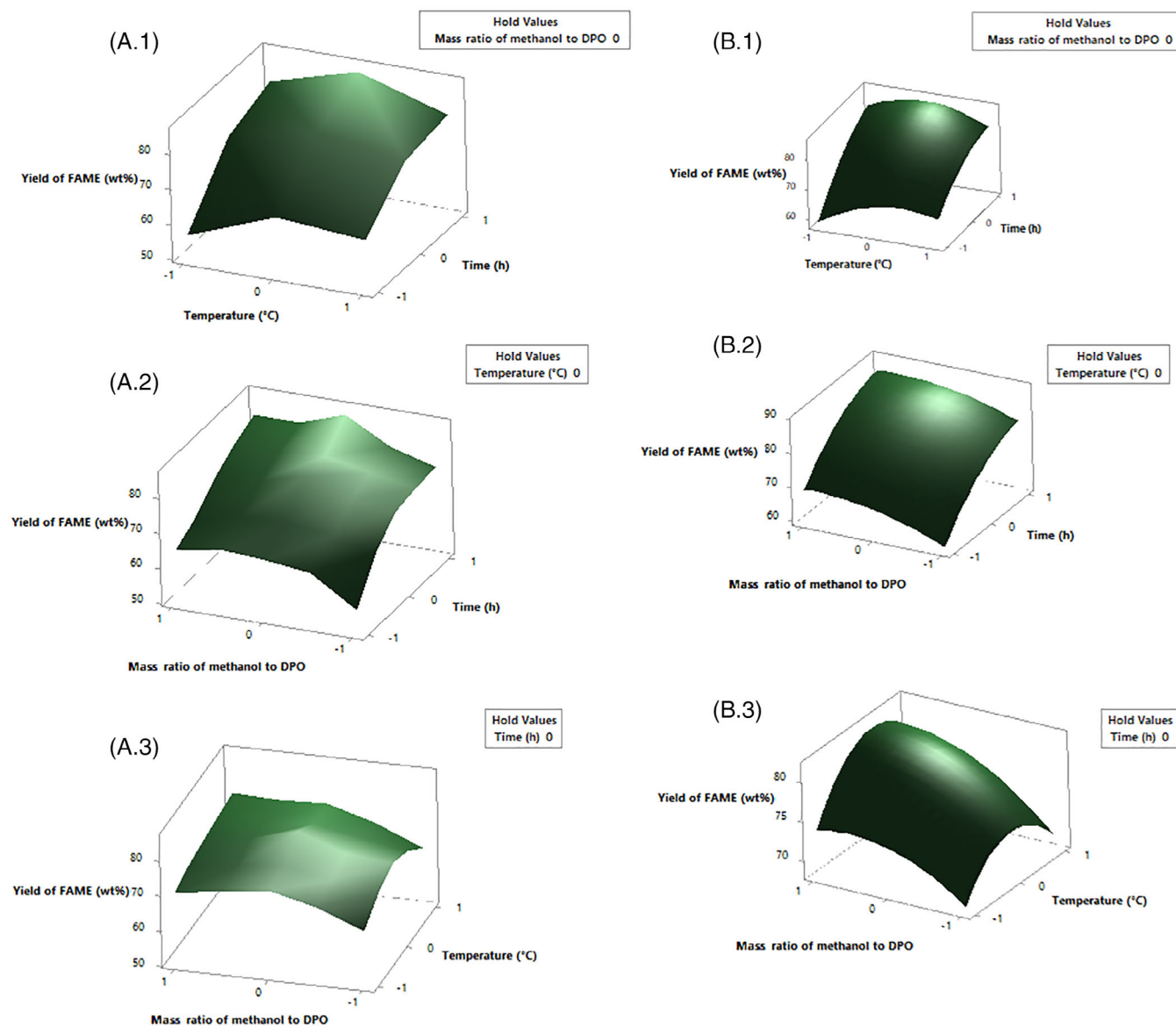


FIGURE 5 The yield of FAME (wt%) based on the A, experimental results and B, predicted results, due to the interaction between (1) reaction time (h) and temperature ($^{\circ}\text{C}$), (2) reaction time (h), and the mass ratio of methanol to DPO, and (3) temperature ($^{\circ}\text{C}$) and the mass ratio of methanol to DPO [Colour figure can be viewed at wileyonlinelibrary.com]

followed by the methanol to DPO mass ratio (C) and reaction temperature (A). The coefficients for the three independent variables (A, B, C) obtained from this plot are 1.58, 9.26, and 3.80, respectively. This coefficient value indicates the sensitivity of the variable. For instance, the coefficient value of reaction time (B, 9.26) pointed out that this variable contributes to the response with the average value of 9.26% when the reaction time is increased by one level. The results obtained from the perturbation plot were also supported by the generated Pareto chart (Figure 6B). As seen from the figure, the significance order of all the linear, quadratic and two-way interaction terms can be sorted into the following sequence: reaction time (B) > mass ratio of methanol to DPO (C) > quadratic temperature (A^2)

> temperature/time (AB) > quadratic reaction time (B^2) > temperature (A) > quadratic mass ratio of methanol to DPO (C^2) > temperature/mass ratio of methanol to DPO (AC). These parameters contribute to the suitability of the mathematical regression model. By inserting all the significant coefficient values to Equation (5), the mathematical model can be expressed as follows:

$$Y = 79.95 + 1.58A + 9.26B + 3.80C - 4.84A^2 - 3.72B^2 - 2.33C^2 - 2.08AB + 1.10AC \quad (5)$$

where Y is the yield of FAME (wt%), and A, B, C are the encoded level of input variables (-1, 0, 1).

TABLE 4 The estimated regression coefficient and their significance for the calculation of FAME yield, generated by ANOVA

Term	Coef	SE Coef	T-value	P-value
Constant	79.947	0.336	238.14	0.000
A	1.583	0.315	5.03	0.001
B	9.262	0.315	29.45	0.000
C	3.805	0.344	11.07	0.000
A ²	-4.842	0.648	-7.48	0.000
B ²	-3.717	0.648	-5.74	0.000
C ²	-2.333	0.746	-3.13	0.011
AB	-2.078	0.352	-5.91	0.000
AC	1.097	0.352	3.12	0.011
BC	-0.550	0.352	-1.56	0.149

The goodness-of-fit analysis for the regressed equation is summarized in Table 5. Based on the ANOVA, the regressed mathematical model shows significance, indicating that the model can be used for predicting the yield of FAME. The low value of SD (0.9947) further points out that most of the experimental data approaching the statistical average.⁵⁰ Figure 6C also observes a well-behaved residual vs predicted plot, indicating that the linear correlation is reasonable. The horizontal band around the zero-line formed by the residuals, without any value stood out from the basic random pattern also suggests that the variances of the error terms are equal and there are no outliers. The lack-of-fit test shows that the *P*-value of the model is 0.3625, emphasizing that the derived equation is well-fitted to the actual data and the discrepancy of the model shows no significance. The value of R-squared for the model is found to be 0.9934, implying that 99.34% of the experimental data can be adequately interpreted by Equation (5). A good agreement between the predicted and experimental response of FAME yield is also observed from the value of adjusted and predicted R-squared which are also close to unity (0.9875 and 0.9656, respectively). This result indicates that the model is sufficient to support the prediction of new responses within the tested range. Furthermore, two other parameters, for example, the coefficient of variation and adequate precision, are also monitored through the ANOVA. Table 5 presents that the values of C.V. and adequate precision are obtained at 1.34% and 46.3751, respectively. While C.V. is used to express the model reproducibility and has a maximum value of 10%, the adequate precision shows the signal-to-noise ratio, which can be used to compare the range of the predicted values at the design points to the average prediction error, with the optimal value of >4.0. Based on the obtained value of

C.V. (1.34%) and adequate precision (46.3751), it can be concluded that the level of data clarity is high and the experimental values are sufficient; indicating that the regressed model can be used to represent all the independent variance assumption.

Meanwhile, the optimum operating condition for the in-situ esterification/transesterification reaction using Cu/DS-HMS-NH₂ is obtained using Minitab (version 18.1) (Figure 7): temperature of 55.3°C (coded level of 0.0303), the reaction time of 5 h (coded level of 1) and methanol to DPO mass ratio of 5.3:1 (coded level of 0.6970). The predicted FAME yield under this optimum condition is monitored at 86.63% with model desirability of 1.00.

Three replicated experiments were performed using these optimum variables to confirm the plausibility of the developed mathematical model. The experimental FAME yield obtained at the optimum operating condition is found at 87.14 ± 0.11 wt% with the FAME purity of 98.45 ± 0.67 wt%. With the error between the experimental and predicted values of only 0.51%, we can conclude that adequate accuracy in the determination of FAME yield using the operating parameters within the tested levels can be achieved via the established equation. The optimum yield of FAME also shows that Cu/DS-HMS-NH₂ is comparable to the existing catalysts published in the literature. Xie and Wan (2019)¹² studied that the oil conversion of 95.8 wt% was achieved only after a 6 h reaction at a temperature of 110°C using the POM-based sulfonated ionic liquid immobilized-UiO-66-2COOH metal-organic framework, while da Conceição et al (2016)¹⁵ presented the use of extreme temperature and catalyst loading (250°C and 30 wt%) to attain 99.2 wt% FAME yield using sulfated niobium oxide. High reaction temperature (200°C) and catalyst loading (7.5 wt%) was also reported by García-Sancho et al (2011)²⁰ to obtain a 95 wt% biodiesel conversion using niobium-impregnated MCM-41 catalyst. Moreover, Omar and Amin (2011)¹¹ mentioned that the transesterification of waste cooking oil in the presence of alkaline-modified zirconia catalyst requires a temperature of 115.5°C to achieve less than 80 wt% FAME yield. Therefore, the mild temperature (55°C), moderate catalyst loading (5 wt%), and comparable reaction time (5 h) obtained from this optimization study are highly favorable since the three parameters are directly related to the process efficiency in the industries.

Table 6 presents the characteristics of the final FAME product. The results show that its fuel properties are following the standard of ASTM D6751. The measured heating value (45.72 MJ/kg) is also within the range observed in the common petrodiesel fuel (42-46 MJ/kg).⁵¹ We observe a similar profile in the FTIR spectra of

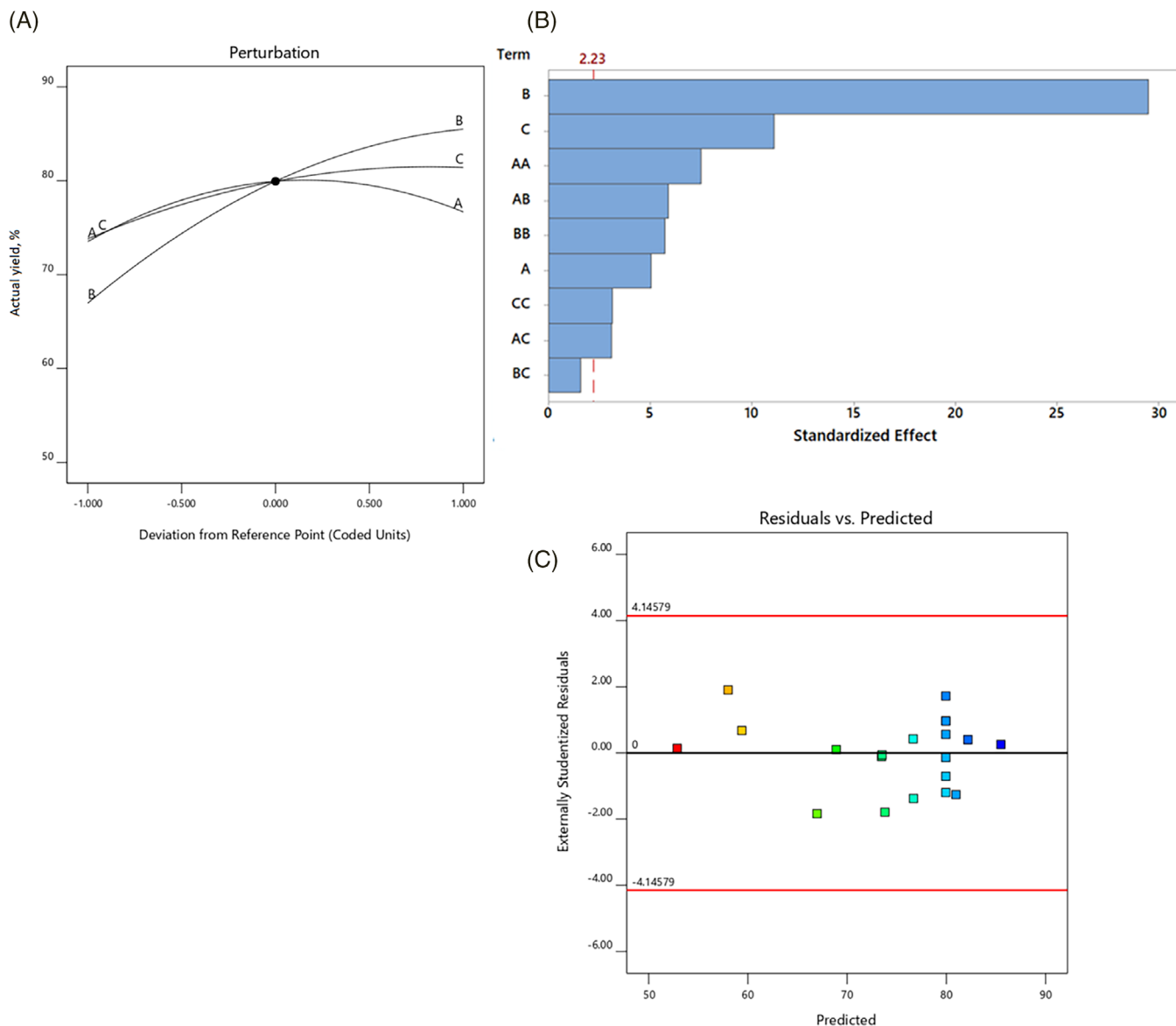


FIGURE 6 A, Perturbation plot and B, Pareto chart showing the significance order of various reaction variables, where A = temperature ($^{\circ}\text{C}$), B = reaction time (h), C = mass ratio of methanol to DPO; and C, the residual vs predicted plot [Colour figure can be viewed at wileyonlinelibrary.com]

DPO and FAME (Figure 8). Several functional groups, for example, the bending vibrations of $-\text{CH}$, $-\text{CH}_2$, $-\text{CH}_3$ (1395 , 1187 , and 760 cm^{-1} for DPO and 1395 , 1181 , and 754 cm^{-1} for FAME), their respective stretching bands (3024 , 2953 , and 2876 cm^{-1} for DPO and 3030 , 2929 , and 2858 cm^{-1} for FAME), carbonyl ($\text{C}=\text{O}$, 1786 cm^{-1} for DPO and 1756 cm^{-1} for FAME), C–O stretching band (1140 cm^{-1} for DPO and 1134 cm^{-1} for FAME) are monitored in both spectra. Fadhil (2021)⁵² also reported similar spectra for bio-oil from the non-edible feedstock, indicating that oils and fats generally consist of the same functional groups. However, the FTIR spectra of FAME show a new signal at 1465 cm^{-1} which indicates the presence of the ester group with its deformation vibration.

This implies that FAME is formed during the simultaneous esterification/transesterification reaction. Moreover, using the external standard pack (47 885 U, containing 37 components FAME standard mix), 11 FAME peaks, including C11:0, C14:1, C15:1, C16:0, C16:2, C18:0, C18:1n9c, C18:1n9t, C18:2, C18:3, C20:0, and C20:3n6, are identified.

3.4 | Reusability study of Cu/DS-HMS-NH₂

To determine the reusability of Cu/DS-HMS-NH₂, several reaction cycles were conducted in series using the

TABLE 5 The ANOVA results for the fitted regression model

Source	Sum of squares	DF	Mean square	F-value	P-value	Remarks
Model	1497.29	9	166.37	168.16	<0.0001	
A	25.06	1	25.06	25.33	0.0005	Significant
B	857.85	1	857.85	867.09	<0.0001	Significant
C	121.19	1	121.19	122.50	<0.0001	Significant
A ²	55.30	1	55.30	55.89	<0.0001	Significant
B ²	32.59	1	32.59	32.94	0.0002	Significant
C ²	9.67	1	9.67	9.78	0.0108	Significant
AB	34.53	1	34.53	34.90	0.0001	Significant
AC	9.64	1	9.64	9.74	0.0109	Significant
BC	2.42	1	2.42	2.45	0.1489	Not significant
Residuals	9.89	10	0.9893			
Lack of fit	4.63	4	1.16	1.32	0.3625	Not significant
Pure error	5.27	6	0.8778			
Total	1507.18	19				
R-squared (R ²)	0.9934	Adjusted R ²	0.9875	Predicted R ²	0.9656	
Adequate precision	46.3751	Coefficient of variation (C.V., %)	1.34	SD	0.9947	

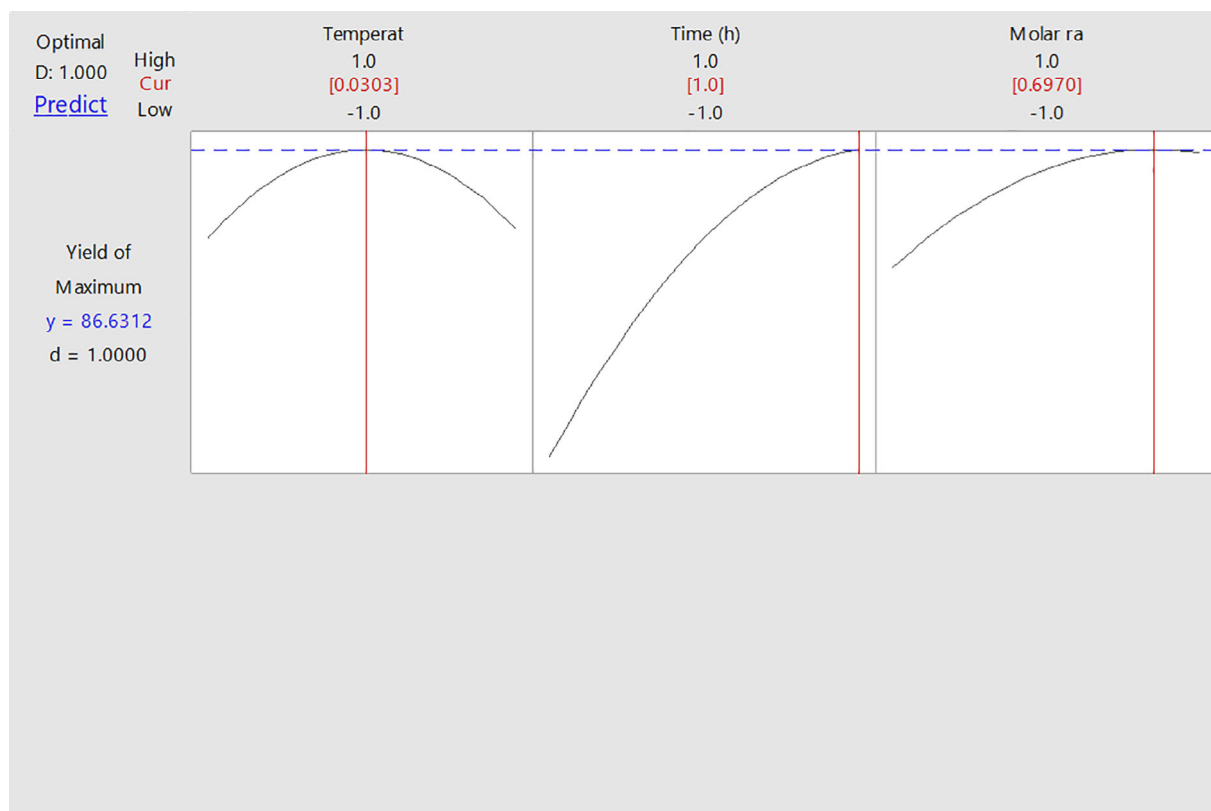


FIGURE 7 Response optimization plot of the three independent variables for the in-situ esterification/transesterification reaction using Cu/DS-HMS-NH₂ [Colour figure can be viewed at wileyonlinelibrary.com]

following optimum condition: temperature = 55.3°C, reaction time = 5 h, and methanol to DPO mass ratio = 5.3:1.

Figure 9 presents the catalytic ability of the reused Cu/DS-HMS-NH₂. Notable from the figure, this catalyst can

TABLE 6 The characteristics of the resulting FAME product

Properties	Methods	Unit	Final FAME product	ASTM D6751
Kinematic viscosity (at 40°C)	ASTM D445	mm ² /s	3.54	1.9-6.0
Flashpoint	ASTM D93	°C	168.4	93 min
Cetane number	ASTM D613	-	53.2	47 min
FAME content (purity)	EN 14103	wt%	98.45	-
Acid value	ASTM D664	mg KOH/g	0.27	0.5 max
Monoglycerides content	ASTM D6584	wt%	0.32	0.4 max
Diglycerides content	EN14105	wt%	0.09	-
Triglycerides content	EN14105	wt%	0.09	-
Calorific value	ASTM D240	MJ/kg	45.72	-

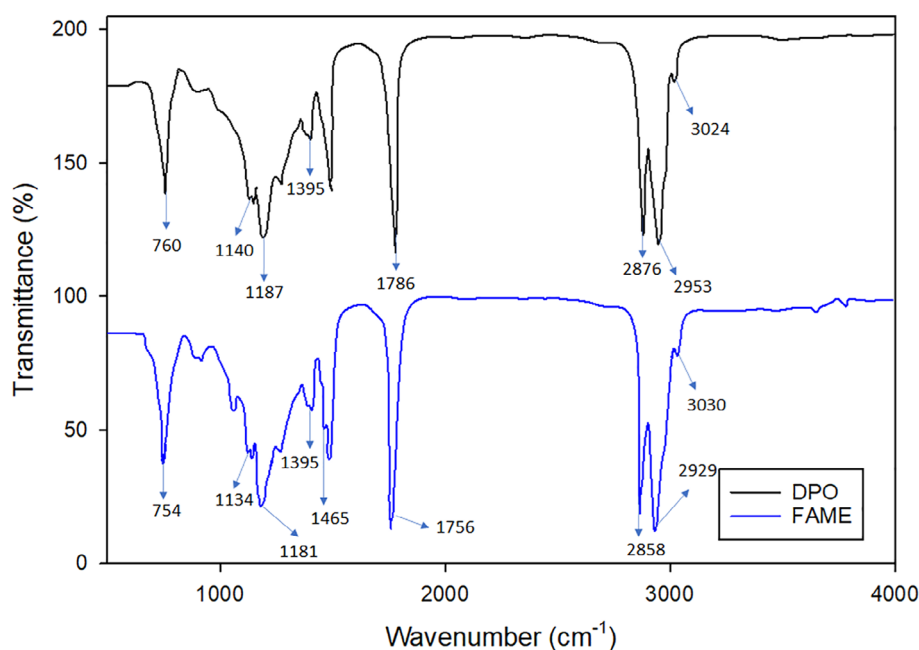
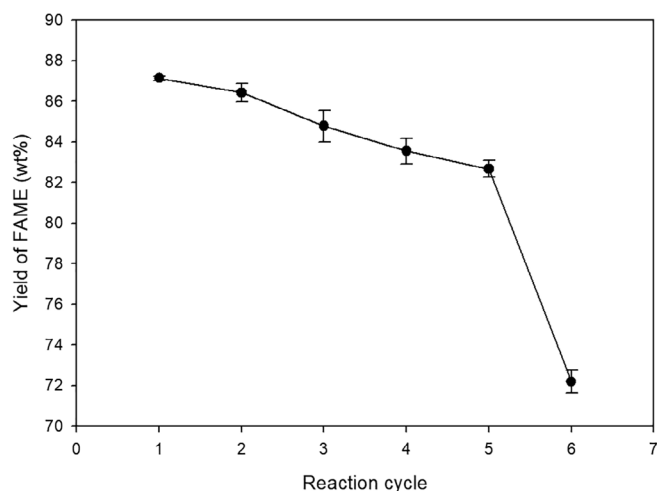


FIGURE 8 The FTIR spectra of DPO and FAME [Colour figure can be viewed at wileyonlinelibrary.com]

FIGURE 9 The catalytic activity of Cu/DS-HMS-NH₂ during the reusability study

maintain the yield of FAME above 80 wt% until the fifth cycle, before significantly drop to 72.18 wt% at the sixth cycle. Similar catalytic performance has been reported for some other solid catalysts, where 5 cycles seem to be the average number in terms of their reusability.^{12,53} The FAME purity for the first five is measured at 97.16 wt%, 97.72 wt%, 98.02 wt%, 97.77 wt%, and 96.94 wt%, respectively; higher than the required ester content in the commercial biodiesel (minimum at 96.5 wt%). The deactivation of Cu/DS-HMS-NH₂ is attributed to the blockage of the catalyst pores by the components present in the reaction system, for example, glycerol, acyl glycerides, and biodiesel.³³ Besides, the FFA content in DPO also contributes to the neutralization of the basic sites in the inner shell of Cu/DS-HMS-NH₂ catalyst,⁵⁴ thereby promoting the production of the amine-carboxylate compound and subsequently, generating emulsion.

3.5 | The catalytic reaction mechanism for the in-situ esterification/transesterification

Figure 10 presents the catalytic reaction mechanism for the in-situ esterification/ transesterification reaction using Cu/DS-HMS-NH₂. As shown in the figure, the outer layer of the catalyst is impregnated by copper (a strong Lewis acid) which was intended to convert FFA to FAME through an esterification process, while the inner shell was functionalized with amine (-NH₂) as

the basic sites to further convert the acyl glycerides to FAME through the process of transesterification.

The in-situ esterification/transesterification mechanism using the Cu/DS-HMS-NH₂ catalyst can be described as follows: all reactant molecules, including acyl glycerides, FFA, and methanol migrate onto the boundary layer of the catalyst and diffuse through the layer onto the outer shell of the catalyst, which is impregnated by the copper. In this layer, the pi carbonyl bond in FFA resonates and undergoes electron

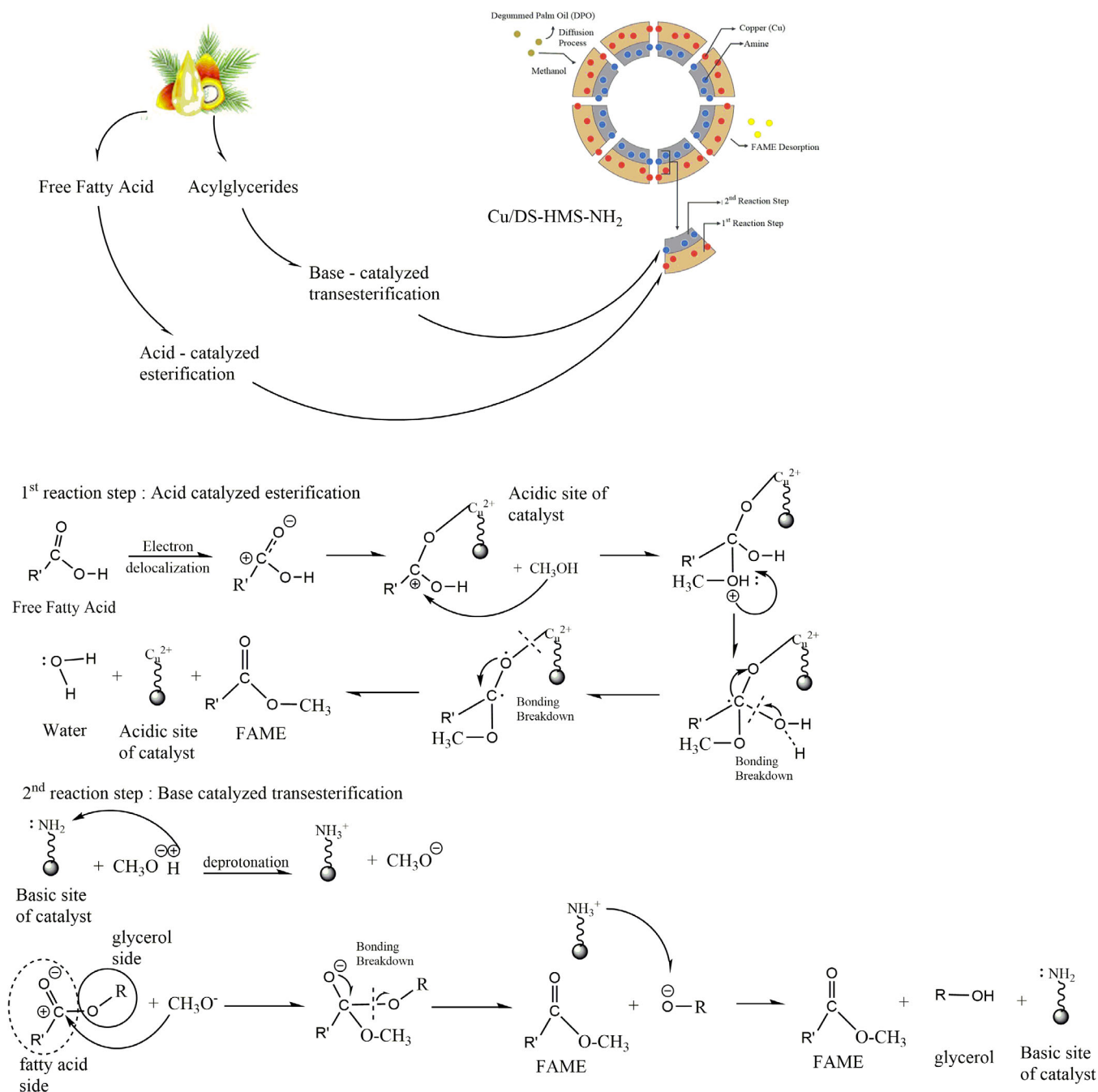


FIGURE 10 The in-situ esterification/transesterification reaction mechanism using Cu/DS-HMS-NH₂ [Colour figure can be viewed at wileyonlinelibrary.com]

delocalization to form carbocation and carbanion,^{55,56} which are highly reactive. The pi carbonyl bond has a weak molecular interaction due to the distance between the electron in the carbanion and the positively charged atomic nucleus (carbocation).⁵⁷ As a result, the copper impregnated on the Cu/DS-HMS-NH₂ catalysts acts as a proton donor and binds the carbanion to form a complex by holding the excess electron density; therefore, stabilize the charge and promote the next reaction step to occur. The chemical interaction in the outer shell continues when the lone pair in the hydroxyl group of methanol, which possesses the electronegative properties, binds to the carbocation, resulting in the release of the hydrogen atom in the hydroxyl group of methanol, further driving the atom to move to the hydroxyl group of FFA. Due to the addition of the attached hydrogen atom, another electron delocalization occurs to adjust the distribution of electrons in the hydroxyl group of FFA. Subsequently, the hydrogen atom attached to the hydroxyl group of FFA is released to form H₂O, followed by the release of the copper complex bond to form the final product in the form of FAME.

Meanwhile, the acyl glycerides diffuse further to the basic sites contained in the inner shell of the catalyst to engage in a transesterification reaction. Initially, methanol undergoes a deprotonation reaction to give the hydrogen atom to the amine group of the catalyst. This reaction results in two products, namely NH₃⁺-embedded catalyst and the alkoxy (RO-) group of methanol. Then, in one of its pi-carbonyl bonds, the acyl glycerides encounter an electron delocalization to form carbocation and carbanion. The alkoxy (RO-) group of methanol is then bound to the carbocation. A further electron resonance occurs to produce a complex of FAME and glycerol. To create a stable compound, the positively charged NH₃⁺ in the catalyst donates the hydrogen proton to the complex of FAME and glycerol to release glycerol from one of the chains⁵⁸ and at the same time, produce FAME as well. Once the reaction is completed, the three products (FAME, H₂O, and glycerol) from the in-situ esterification/transesterification reaction are subsequently desorbed to the surface of the catalyst.

4 | CONCLUSION

Cu/DS-HMS-NH₂ is successfully fabricated and employed to promote the in-situ esterification/transesterification reaction, for the synthesis of FAME from DPO with high FFA and moisture content. The particle size of the Cu/DS-HMS-NH₂ catalyst is uniform at 157 nm with a hollow core size of 81 nm. This catalyst consists of 2 layers with a similar thickness of 16-19 nm. The textural

properties of Cu/DS-HMS-NH₂ are also comparable to the existing heterogeneous catalyst, with S_{BET} of 733.24 m²g⁻¹, and V_p of 0.54 cm³g⁻¹. The maximum FAME yield at 87.14 ± 0.11 wt% with the purity of 98.45 ± 0.67 wt% was obtained using Cu/DS-HMS-NH₂ under the following optimum condition: 55.3°C, 5 h, methanol to DPO mass ratio of 5.3:1, and 5 wt% catalyst loading, indicating the high catalytic activity of Cu/DS-HMS-NH₂. The result of the statistical ANOVA shows that the reaction time gives the most significant influence on the yield of FAME, followed successively by the mass ratio of methanol to DPO and temperature. The predicted and experimental results have a direct proportional output, as shown by the goodness of fit analysis. Based on the reusability study, the catalyst produces a high yield of FAME (>80 wt%) until the fifth cycle. Therefore, Cu/DS-HMS-NH₂ can be considered as a promising solid catalyst to prepare biodiesel from low-quality oils.

ACKNOWLEDGEMENTS

The authors thank Professor Chun-Hu Chen, National Sun Yat-Sen University, and National Taiwan University of Science and Technology, for providing the facilities for material characterizations. This work was supported by Widya Mandala Surabaya Catholic University, through the research grant no. 2263/WM01/N/2020.

DATA AVAILABILITY STATEMENT

The data that support the findings of this study are available from the corresponding author upon reasonable request.

ORCID

Maria Yuliana  <https://orcid.org/0000-0002-3915-9401>

REFERENCES

1. Gurunathan B, Ravi A. Biodiesel production from waste cooking oil using copper doped zinc oxide nanocomposite as heterogeneous catalyst. *Bioresour Technol.* 2015;188:124-127.
2. Adhari H, Yusnimar Y, Utami SP. Pemanfaatan minyak jelantah menjadi biodiesel dengan katalis zno presipitan zinc karbonat: pengaruh waktu reaksi dan jumlah katalis. *J Online Mahasiswa.* 2016;3:1-7.
3. Puna JF, Gomes JF, Correia MJN, Soares Dias AP, Bordado JC. Advances on the development of novel heterogeneous catalysts for transesterification of triglycerides in biodiesel. *Fuel.* 2010; 89:3602-3606.
4. Chaudhary S, Milton MD, Garg P. A base- and metal-free protocol for the synthesis of 2-aryl/heteroaryl Thiazolines. *Chem Sel.* 2017;2:650-654.
5. Samart C, Chaiya C, Reubroycharoen P. Biodiesel production by methanolysis of soybean oil using calcium supported on mesoporous silica catalyst. *Energy Convers Manag.* 2010;51: 1428-1431.

6. Jacobson K, Gopinath R, Meher LC, Dalai AK. Solid acid catalyzed biodiesel production from waste cooking oil. *Appl Catal B Environ*. 2008;85:86-91.
7. Xie W, Yang X, Fan M. Novel solid base catalyst for biodiesel production: mesoporous SBA-15 silica immobilized with 1,3-dicyclohexyl-2-octylguanidine. *Renew Energy*. 2015;80:230-237.
8. Pangestu T, Kurniawan Y, Soetaredjo FE, et al. The synthesis of biodiesel using copper based metal-organic framework as a catalyst. *J Environ Chem Eng*. 2019;7:103277.
9. Zhou K, Chaemchuen S. Metal-organic framework as catalyst in esterification of oleic acid for biodiesel production. *Int J Environ Sci Dev*. 2017;8:251-254.
10. Chen S-Y, Mochizuki T, Abe Y, Toba M, Yoshimura Y. Ti-incorporated SBA-15 mesoporous silica as an efficient and robust Lewis solid acid catalyst for the production of high-quality biodiesel fuels. *Appl Catal B Environ*. 2014;148-149:344-356.
11. Omar WNNW, Amin NAS. Biodiesel production from waste cooking oil over alkaline modified zirconia catalyst. *Fuel Process Technol*. 2011;92:2397-2405.
12. Xie W, Wan F. Immobilization of polyoxometalate-based sulfonated ionic liquids on UiO-66-2COOH metal-organic frameworks for biodiesel production via one-pot transesterification-esterification of acidic vegetable oils. *Chem Eng J*. 2019;365:40-50.
13. Boz N, Degirmenbasi N, Kalyon DM. Esterification and transesterification of waste cooking oil over Amberlyst 15 and modified Amberlyst 15 catalysts. *Appl Catal B Environ*. 2015;165:723-730.
14. Liu H, Chen J, Chen L, Xu Y, Guo X, Fang D. Carbon nanotube-based solid sulfonic acids as catalysts for production of fatty acid methyl Ester via transesterification and esterification. *ACS Sustain Chem Eng*. 2016;4:3140-3150.
15. da Conceição LRV, Carneiro LM, Rivaldi JD, de Castro HF. Solid acid as catalyst for biodiesel production via simultaneous esterification and transesterification of macaw palm oil. *Ind Crop Prod*. 2016;89:416-424.
16. Li Y, Zhang XD, Sun L, Xu M, Zhou WG, Liang XH. Solid superacid catalyzed fatty acid methyl esters production from acid oil. *Appl Energy*. 2010;87:2369-2373.
17. Li Y, Shi J. Hollow-structured mesoporous materials: chemical synthesis, functionalization and applications. *Adv Mater*. 2014;26:3176-3205.
18. Stein A. Advances in microporous and mesoporous solids - highlights of recent progress. *Adv Mater*. 2003;15:763-775.
19. Ying JY, Mehnert CP, Wong MS. Synthesis and applications of supramolecular-templated mesoporous materials. *Angew Chem Int Ed*. 1999;38:56-77.
20. García-Sancho C, Moreno-Tost R, Mérida-Robles JM, Santamaría-González J, Jiménez-López A, Maireles-Torres P. Niobium-containing MCM-41 silica catalysts for biodiesel production. *Appl Catal B Environ*. 2011;108-109:161-167.
21. Chang F, Yan C, Zhou Q. Synthesis of a new copper-based supramolecular catalyst and its catalytic performance for biodiesel production. *Int J Chem Eng*. 2018;2018:1-8.
22. Fadhil AB, Saeed IK, Saeed LI, Altamer MH. Co-solvent ethanolysis of chicken waste: optimization of parameters and characterization of biodiesel. *Energy Sour Part A*. 2016;38:2883-2890.
23. Santosa FH, Laysandra L, Soetaredjo FE, Santoso SP, Ismadji S, Yuliana M. A facile noncatalytic methyl ester production from waste chicken tallow using single step subcritical methanol: optimization study. *Int J Energy Res*. 2019;43:8852-8863.
24. Lie J, Rizkiana MB, Soetaredjo FE, Ju YH, Ismadji S, Yuliana M. Non-catalytic transesterification of waste cooking oil with high free fatty acids content using subcritical methanol: process optimization and evaluation. *Waste Biomass Valorization*. 2020;11:5771-5781.
25. Yuliana M, Santoso SP, Soetaredjo FE, et al. A one-pot synthesis of biodiesel from leather tanning waste using supercritical ethanol: process optimization. *Biomass Bioenergy*. 2020;142:105761.
26. Lee HV, Yunus R, Juan JC, Taufiq-Yap YH. Process optimization design for jatropha-based biodiesel production using response surface methodology. *Fuel Process Technol*. 2011;92:2420-2428.
27. Wang J, Liu C, Tong L, et al. Iron-copper bimetallic nanoparticles supported on hollow mesoporous silica spheres: an effective heterogeneous Fenton catalyst for orange II degradation. *RSC Adv*. 2015;5:69593-69605.
28. You C, Yu C, Yang X, et al. Double-shelled hollow mesoporous silica nanospheres as an acid-base bifunctional catalyst for cascade reactions. *New J Chem*. 2018;42:4095-4101.
29. Zaidi HA, Pant KK. Catalytic activity of copper oxide impregnated HZSM-5 in methanol conversion to liquid hydrocarbons. *Can J Chem Eng*. 2008;83:970-977.
30. Das SK, Bhunia MK, Sinha AK, Bhaumik A. Self-assembled mesoporous zirconia and sulfated zirconia nanoparticles synthesized by triblock copolymer as template. *J Phys Chem C*. 2009;113:8918-8923.
31. Tsou CJ, Hung Y, Mou CY. Hollow mesoporous silica nanoparticles with tunable shell thickness and pore size distribution for application as broad-ranging pH nanosensor. *Microporous Mesoporous Mater*. 2014;190:181-188.
32. Khatun R, Bhanja P, Mondal P, Bhaumik A, Das D, Manirul IS. Palladium nanoparticles embedded over mesoporous TiO₂ for chemical fixation of CO₂ under atmospheric pressure and solvent-free conditions. *New J Chem*. 2017;41:12937-12946.
33. Suryajaya SK, Mulyono YR, Santoso SP, et al. Iron (II) impregnated double-shelled hollow mesoporous silica as acid-base bifunctional catalyst for the conversion of low-quality oil to methyl esters. *Renew Energy*. 2021;169:1166-1174.
34. Klinghoffer NB, Castaldi MJ, Nzihou A, et al. Catalyst Properties and catalytic performance of char from biomass gasification to cite this version: HAL id: HAL-01632400 catalyst Properties and catalytic performance of char from biomass Gasification. *Ind Eng Chem Res*. 2012;51:13113-13122.
35. Zakeri M, Samimi A, Shafiee Afarani M, Salehirad A. Effects of porosity and pore size distribution on mechanical strength reliability of industrial-scale catalyst during preparation and catalytic test steps. *Part Sci Technol*. 2018;36:96-103.
36. Peng W, Zhang Z, Rong M, Zhang M. Core-shell structure design of hollow mesoporous silica nanospheres based on thermo-sensitive PNIPAM and pH-responsive catechol-Fe³⁺ complex. *Polymers*. 2019;11:1832.
37. Baskar G, Soumiya S. Production of biodiesel from castor oil using iron (II) doped zinc oxide nanocatalyst. *Renew Energy*. 2016;98:101-107.

38. Cai J, Zhang QY, Wei FF, et al. Preparation of copper (II) containing Phosphomolybdic acid salt as catalyst for the synthesis of biodiesel by esterification. *J Oleo Sci.* 2018;67: 427-432.
39. Ong HR, Khan MR, Chowdhury MNK, Yousuf A, Cheng CK. Synthesis and characterization of CuO/C catalyst for the esterification of free fatty acid in rubber seed oil. *Fuel.* 2014;120: 195-201.
40. Amalia Kartika I, Yani M, Ariono D, Evon P, Rigal L. Biodiesel production from jatropha seeds: solvent extraction and in situ transesterification in a single step. *Fuel.* 2013;106:111-117.
41. Wei Z, Xu C, Li B. Application of waste eggshell as low-cost solid catalyst for biodiesel production. *Bioresour Technol.* 2009; 100:2883-2885.
42. Alenezi R, Leeke GA, Winterbottom JM, Santos RCD, Khan AR. Esterification kinetics of free fatty acids with supercritical methanol for biodiesel production. *Energy Convers Manag.* 2010;51:1055-1059.
43. Farooq M, Ramli A. Biodiesel production from low FFA waste cooking oil using heterogeneous catalyst derived from chicken bones. *Renew Energy.* 2015;76:362-368.
44. Canakci M, Van Gerpen J. Biodiesel production via acid catalysis. *Trans Am Soc Agric Eng.* 1999;42:1203-1210.
45. Farooq M, Ramli A, Subbarao D. Biodiesel production from waste cooking oil using bifunctional heterogeneous solid catalysts. *J Clean Prod.* 2013;59:131-140.
46. Liu S, Wang Y, Oh JH, Herring JL. Fast biodiesel production from beef tallow with radio frequency heating. *Renew Energy.* 2011;36:1003-1007.
47. Madhuvilakku R, Piraman S. Biodiesel synthesis by TiO₂-ZnO mixed oxide nanocatalyst catalyzed palm oil transesterification process. *Bioresour Technol.* 2013;150:55-59.
48. Yin X, Duan X, You Q, Dai C, Tan Z, Zhu X. Biodiesel production from soybean oil deodorizer distillate using calcined duck eggshell as catalyst. *Energy Convers Manag.* 2016;112: 199-207.
49. Gunawan F, Kurniawan A, Gunawan I, et al. Synthesis of biodiesel from vegetable oils wastewater sludge by in-situ subcritical methanol transesterification: process evaluation and optimization. *Biomass Bioenergy.* 2014;69:28-38.
50. Balajii M, Niju S. A novel biobased heterogeneous catalyst derived from *Musa acuminata* peduncle for biodiesel production – process optimization using central composite design. *Energy Convers Manag.* 2019;189:118-131.
51. Association WN. Heat values of various fuels. 2018. Available at: <http://www.world-nuclear.org/information-library/facts-and-figures/heat-values-of-various-fuels.aspx>.
52. Fadhil AB. Production and characterization of liquid biofuels from locally available nonedible feedstocks. *Asia Pac J Chem Eng.* 2021;16:1-21.
53. Ullah Z, Bustam MA, Man Z. Biodiesel production from waste cooking oil by acidic ionic liquid as a catalyst. *Renew Energy.* 2015;77:521-526.
54. Kouzu M, Hidaka JS. Transesterification of vegetable oil into biodiesel catalyzed by CaO: a review. *Fuel.* 2012;93:1-12.
55. Herges R, Geuenich D. Delocalization of electrons in molecules. *Chem Eur J.* 2001;105:3214-3220.
56. Peter K Vollhardt C. NES. Organic Chemistry; Palgrave version: Structure and Function. 2014.
57. Deen MJ, Pascal F. Springer handbook of electronic and photonic materials. *J Mater Sci Mater Electron.* 2007;17:549-575.
58. Trejo-Zárraga F, Hernández-Loyo F, Chavarría-Hernández J, Sotelo-Boyás R. Kinetics of transesterification processes for biodiesel production. In: Biernat K, ed. *Biofuels - State of Development.* London, United Kingdom: Intechopen; 2018.

How to cite this article: Rahadi AN, Martinus JJ, Santoso SP, et al. Double-shelled hollow mesoporous silica incorporated copper (II) (Cu/DS-HMS-NH₂) as a catalyst to promote in-situ esterification/transesterification of low-quality palm oil. *Int J Energy Res.* 2021;1-18. <https://doi.org/10.1002/er.7064>